CHEMICAL ENGINEERING TRANSACTIONS
VOL. 47, 2016
A publication of AIDIC
The Italian Association of Chemical Engineering
Online at www.aidic.it/cet
Guest Editors: Angelo Chianese, Luca Di Palma, Elisabetta Petrucci, Marco Stoller

ISBN 978-88-95608-38-9; **ISSN** 2283-9216
DOI: 10.3303/CET1647054

Synthesis and Functionalization of Carbon Nanotubes and Graphene Based Supercapacitor for Arsenic Removal and Water Desalination: a Comparison

Maria Sarno, Alfonso Troisi*, Carmela Scudieri, Paolo Ciambelli

Department of Industrial Engineering and Centre NANO_MATES University of Salerno
Via Giovanni Paolo II ,132 - 84084 Fisciano (SA), Italy
alfonsotroisi10@yahoo.it

In this paper, we report a systematic comparison of carbon nanotubes (CNTs) and graphene oxide (GO) adsorption and desalination efficiency at different oxidation level under electrochemical conditions. Particular care has been devoted to the evaluation of the energy storage performance, through a comparison with the capacitive behavior in a typical aqueous electrolyte, a solution 1M of H_2SO_4. The specific capacitance calculated from the Cyclic Voltammetry (CV) curve at 2mV/sec for as produced purified CNTs (CNTp), highly hydrophilic CNTs (CNTf), partially reduced CNTf (CNTftt) and GO in H_2SO_4 are respectively 160 F/g, 356 F/g, 298 F/g and 145 F/g. We evaluate for our nanomaterials high capacitive deionization (CDI), we also demonstrate that although surface functional groups are essential to provide better contact between electrode and electrolyte leading to high capacitance, however a more preserved electrical structure allows to obtain higher performance (e.g. 135 F/g and 185 F/g for CNTf and CNTftt, respectively).

1. Introduction

Heavy metals in water are a major concern because of their toxicity towards aquatic-life, human beings and the environment; the presence of toxic metals in groundwater and seawater sources is an important issue in water and wastewater treatment, as their effects on human health are well established. Among toxic metals, a check on arsenic contamination of natural water sources has been recorded by World Health Organization as a first priority issue; it is classified as one of the most toxic and carcinogenic elements. Seawater is the major source of water on Earth, commercially feasible technology is in demand for desalinating seawater with low energy loss.

The simplicity of a capacitive deionization (CDI) recently triggered a significant interest to this approach as an alternative to other techniques (e.g. reverse osmosis…) for both static and mobile water desalination and purification application. CDI is an emerging technique (Porada et al., 2013) for removing dissolved, charged species from aqueous solutions, and has been previously applied to brackish water desalination, sea water desalination, wastewater remediation, and water softening. The past decade has seen a remarkable number of innovations in the exponentially growing field of CDI, accompanied by the growing commercial development of products utilizing CDI technology by various companies around the globe. A CDI cell consists of a pair of porous electrodes, typically carbon made; the salt ions present in the feed migrate into electrical double layers (EDLs) along the pore surfaces at the carbon/water interface, removing salt from the feed water (a process known as ‘‘electrosorption’’). Salt ions are electrostatically held in the double layer until the discharging step, where the external power supply is shorted or its polarity reversed. During discharge the release of ions results in a brine stream, and the charge leaving the cell can be leveraged to recover energy (analogously to the energy from a discharging electric capacitor). As a salt ion removal technology, CDI provides several unique advantages. Firstly, CDI enables salt removal at low (sub-osmotic) pressure and room temperature, with the primary input being a small cell voltage and an electric current whose magnitude depends on the system size. Thus, unlike reverse osmosis or distillation-based desalination systems, CDI does not need to be coupled to high pressure pumps or heat sources, allowing for facile system scaling up. It does not require an

Please cite this article as: Sarno M., Troisi A., Scudieri C., Ciambelli P., 2016, Synthesis and functionalization of carbon nanotubes and graphene based supercapacitor for arsenic removal and water desalination: a comparison, Chemical Engineering Transactions, 47, 319-324 DOI: 10.3303/CET1647054

installation of a large, heavy and expensive high pressure system. Secondly, CDI can work at lower salt concentration than reverse osmosis (Zhao et al., 2013). Thirdly, the operating principle of CDI shares many features with electrochemical supercapacitors (Porada et al., 2013), including reversible operation and energy storage capability (CDI can be crudely thought of as ‘‘desalination with a supercapacitor’’). Thus, CDI systems have the unique ability to simultaneously store energy (similarly to a supercapacitor) and purify and desalinate water upon being charged.

With increasing interest in nanotechnology many types of carbons and carbon-based nanomaterials have emerged even for applications such as the treatment and desalination of water. Properties like high surface area, easy chemical or physical modification, tuning of properties for particular applications, and excellent capacity for removal inorganic contaminants, candidate them for novel applications in water treatment.

Few papers have been published to date on this theme. Electrochemical activity of functionalized multiwalled carbon nanotubes (MWNTs) (Mishra et al., 2011a), magnetite/MWNTs composite (Mishra et al. 2010), functionalized graphene (Mishra et al., 2011b), carbon nanotubes-polymer composites (Benson et al., 2013) were analysed for arsenite and arsenate, and NaCl removal by using cyclic voltammetry (CV). Really, there are still many aspects to explore and clarify.

In this paper we present a systematic comparison, based on the arsenic adsorption and water desalination, on high surface area CNTs (mostly single-wall carbon nanotubes (SWNTs)): highly hydrophilic functionalized CNTs and for the first time CNTs covered by mostly –OH groups. Also graphene oxide (GO) was prepared and tested for comparison. Based on a supercapacitive concept, we demonstrate the high electrochemical activity of these nanomaterials toward the removal of arsenite and arsenate ions containing water, as well as for NaCl removal, and the key role of the functional surface groups. Moreover, particular care has been devoted to the evaluation of the energy storage performance, through a comparison with the capacitive behavior in a typical aqueous electrolyte, a solution 1M of H_2SO_4.

2. Experimental Section

2.1 Preparation of CNT. Carbon nanotubes were obtained by methane catalytic chemical vapour deposition (CCVD) (Sarno et al., 2012, Sarno et al., 2013a)**.** Catalyst samples were prepared by wet impregnation of magnesium oxide with cobalt acetate aqueous solution (5 wt %) and drying at 140 °C for 12 h. A gas mixture (500 cm^3/min flow rate of 10% methane in hydrogen) was fed to a continuous flow reactor after heating it from 298K up to 1273K (10K/min) under helium flow. After 10 min the methane–hydrogen flow was stopped, and the reactor was cooled down to room temperature under helium flow. The carbon material grown on the catalyst was recovered by chemical attack with concentrated HCl. Finally, the solid residue, in the following ***CNTp***, was washed by distilled water, centrifuged and dried at 353K for 12h.

2.2 Preparation of functionalized CNTs. Functionalized CNTs were prepared by a modified Hummer’s method; 0.2 g of ***CNTp*** were mixed with 25 ml of H_2SO_4 at 0°C. Then, 2 g of $KMnO_4$ were gradually added under stirring, taking care to keep the temperature below 10°C. The mixture was kept under stirring for two hours in an ice bath, the temperature was then raised to 35°C and held for one hour. Water, 25 ml, was then added to the mixture, ice was used to control exothermic reaction heat. After another hour of stirring, the mixture was brought to a volume of 75 ml with the addition of H_2O to stop the reaction and subsequently 8 ml of H_2O_2 were added to reduce residual $KMnO_4$. The nanomaterial, in the following named ***CNTf***, was then separated by mechanical filtration. Thermal reduction of ***CNTf*** under vacuum, up to 300°C, was applied to reduce the number of functional groups (e.g. –COOH groups were removed, while the other functional groups reduced, temperatures higher than 400 result only in a little survival of phenolic groups (Ganguly et al. 2011)), obtaining a sample named ***CNTftt*** in following.

2.3 Preparation of GO nanosheets. In a typical experiment, 2 g of pure graphite powder were added to 100 ml of H_2SO_4 into 250 ml volumetric flask, and kept under magnetic stirring in ice bathing. Then, 8 g of $KMnO_4$ were added gradually under stirring, maintaining the mixture temperature below 10^o C by cooling. The whole adding procedure should last for more than 1 hour to avoid intense exothermic reaction effects. After 1 h 30 min of mixing the system was heated up to 35-40^o C for 30 min to initiate the oxidation process. During oxidation and intercalation the volume of graphite expanded and viscosity increased. Then, the mixture was diluted with 100 ml of distilled water. Because the addition of water to concentrated sulfuric acid releases a large amount of heat, the addition is performed in an ice bath to keep the temperature below 100^o C. The mixture was stirred for 1 hour and then diluted to approximately 300 ml with water. After that, 20 ml of H_2O_2 were added to the mixture to reduce residual $KMnO_4$. The mixture released a large amount of bubbles and the color turned to a brilliant yellow. Finally, the mixture was washed by centrifugation, repeatedly, to remove metal ions and the acid. The resulting dispersion was dried and a solid graphite oxide (GrO) was obtained. 0.1 g of GrO were put into 100 ml of distilled water, obtaining a good dispersion using a Bath Sonication (15 min)

and a Strong Sonication (5 min at 60% of power amplitude of the ultrasound). In this step the layers of graphite oxide are furtherly exfoliated giving a dispersion of graphene oxide (exfoliated graphite oxide) layers in water. The bigger particles (graphite oxide not completely exfoliated and residual graphite not reacted) are removed from the solution by centrifugation (3 min at 6000 rpm) and the supernatant phase (distilled water + graphene oxide (***GO***)) was recollected.

2.4 Materials characterization. All samples were characterised by numerous techniques. Simultaneous analysis (TGA–DGA) in flowing air was performed with a Thermogravimetric Analyser SDTQ 600 TA Instruments, at 5K/min heating rate. TEM images were obtained with a FEI Tecnai electron microscope operating at 200 kV with a LaB6 filament as the source of electrons. The preparation of samples for TEM analysis involved sonication in ethanol for 2–5 min and deposition on a carbon grid. XRD measurements were performed with a Bruker D8 X-ray diffractometer using CuKα radiation. Surface area and porosity characterisation was obtained by N_2 adsorption–desorption at 77K with a Thermoquest Sorptomatic 1900. Powder samples were outgassed in He flow at 523K for 12h before measurements. FT-IR spectra were acquired by a Vertex 70 Apparatus (Bruker Corporation). For the electrochemical measurements 4 mg of the samples were dispersed in 80 µl of 5 wt.% Nafion solution to form a homogeneous ink. Then the ink was partially drip casted onto a glassy carbon electrode of 3 mm in diameter until to fill. Cyclic Voltammetry (CV) curves were obtained using a potentiostat from Amel Instruments, using saturated calomel as e reference electrode, graphite as counter electrode and loadable glassy carbon as working electrode. The measurements were performed in 1 M H_2SO_4, in 1 M of NaCl solutions and for the arsenic removal tests in a 1 mg/L solution of sodium arsenate dibasic heptahydrate ($Na_2HAsO_4 \cdot 7H_2O$, Sigma-Aldrich, ≥98%) and sodium (meta)arsenite ($NaAsO_2$, Sigma-Aldrich, ≥90%).

3. Results and discussion

3.1 Materials characterization. TEM analysis gives clear evidence that the as synthesized carbon is in the form of nanotubes (typical CNTs image in Figure 1a). They are sinuous and entangled and their size distribution is somewhat narrow. Cobalt nanoparticles are located inside the tubes, generally at their one end. An evaluation of the nanotube inner diameter size suggests that it is quite close is equal to the dimension of these particles, suggesting that it can be controlled by the metal dispersion on the catalyst support (Ciambelli et al., 2005). High resolution TEM analysis allows to measure the geometrical characteristics of the nanotubes, (see Figure 1b of purified CNT), that have an inner mean diameter of 2.5 nm. The TEM analysis shows that the majority of the nanotubes are single-wall (SWNT), together with a small fraction of CNTs with two and up to four layers, (Figure 1b). Transmission Electron Microscopy (TEM) image of the GO is shown in Figure 1c. GO exhibits a rough surface showing wrinkles (Baldino et al., 2015).

The XRD pattern of ***CNTftt*** shows only a broad peak around 2θ=26.0°, due to the distance between adjacent areas of different SWNT and between tube walls for double-walled and multi-walled, which is also indicative of a low degree of order. ***CNTf*** samples, however, exhibit a broader peak, likely due to the higher level of functionalization (***CNTf*** occupied a volume about three times higher than ***CNTftt***) and inferior quality. The XRD pattern of ***GO*** shows the (002) reflection at 2θ=8.9°, that corresponds to a basal spacing of 9.9 Å (Figure 2a). This value can be explained by the hydrophilic character induced by the high oxidation level of ***GO***, favouring the presence of intercalated water molecules between adjacent graphene oxide sheets (values varying form 0.6 nm for dry GO to 1.2 nm for hydrated GO have been previously reported (Baldino et al., 2015).

The Figure 2b reports a comparison of ***CNTftt*** and ***CNTf*** Raman spectra. In particular, the most prominent features of the sp^2 carbon materials, which are known as the G band and the G' band, were observed at 1575 cm^{-1} and approximately 2700 cm^{-1}, respectively, using 514 nm excitation wavelength. A very small D-band due to disorder or edge of a graphite sample can be also seen at about half of the frequency of the G' band (around 1345 cm^{-1}). The ***CNTf*** Raman Spectrum shows a more intense D band, a reduction of the G' line and displays a shift to higher frequencies (blue-shift) of the G band, as it is typical of high functionalization degree (Sarno et al., 2013b). A typical ***GO*** Raman spectrum is also shown in Figure 2b, displaying two prominent peaks at: ~1343 and ~1592 cm^{-1}, that correspond to the well-documented D and G bands, respectively (Baldino et al., 2015). The G band broadens and up-shifts in comparison to those observed in graphite. The I_D/I_G ratio increases with increasing the mean distance between two defects (L_D) from 1 to about 3 nm, in our case the I_D/I_G ratio is 0.71 indicating an L_D of about 1.3 nm. In the spectrum are also visible the 2D peak at 2700 cm^{-1}, and the D+D' peak at 2940 cm^{-1} due to the defect activated combination of phonons.

Figure 2c shows the infrared-absorbance spectrum of our ***GO*** with the typical contributions from hydroxyl (C-OH), ketonic species (C=O), carboxyl (COOH), sp2-hybridized C=C (in-plane vibrations), epoxide (C-O-C) and

various C-O and C=O containing chemical species such as lactol, peroxide, dioxolane, anhydride and cyclic ether, which fall in the three spectral regions labelled α, β and γ characteristic of ether-like and ketone-like species (Acik et al., 2010). We assign the signals between 3600 and 3200 cm^{-1} to the O–H stretching vibration of free water, associated hydroxyl groups in GO and adsorbed water molecules. The signal at 1607 cm^{-1} is related to the skeletal vibration of the C=C bond, while the signal at about 1410 cm^{-1} corresponds to bending in alcoholic groups (C-OH). The peak at 1059 cm^{-1} might also originate from skeletal C–C vibrational modes. Vibrations of C–O of different species mainly epoxy and hydroxyl groups, less evident in the spectrum of ***CNTftt***, are present in the range of 1300 and 800 cm^{-1}. The signals originating from C=O bond of the carboxyl group at about 1724 cm^{-1}can be seen in the spectra of ***CNTf*** and GO, while, as expected, is absent in the spectrum of ***CNTftt***.

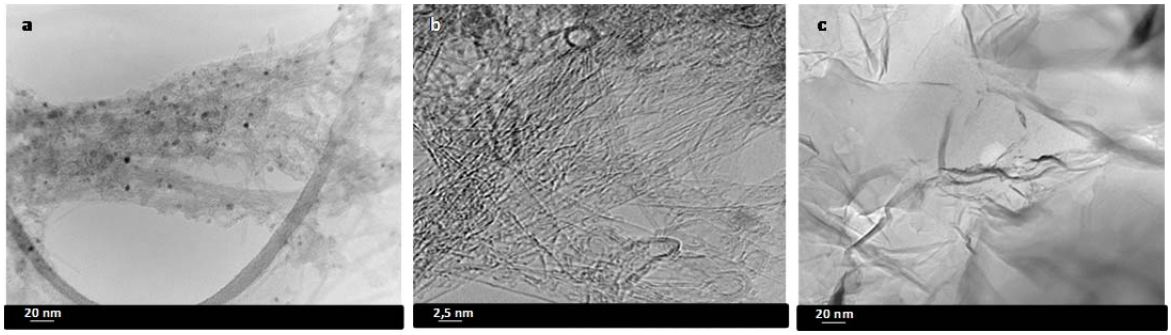

Figure 1 : TEM images of as prepared CNT (a), CNT after purification (b), GO (c).

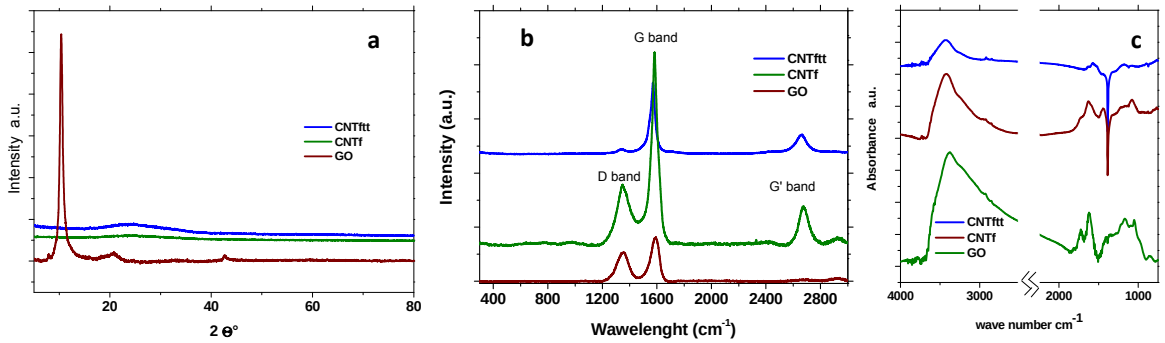

*Figure 2: XRD patterns (a) Raman Spectra (b) and FT-IR analysis (c) of **CNTftt**, **CNTf** and **GO**.*

3.2 Electrochemical characterization

In order to evaluate the electrochemical properties cycling voltammetry (CV) was performed. As an example, the CV curves at 2-10-20-50-100 mV/s, in the potential window of 0-1 V in 1M H_2SO_4 electrolyte, are presented in Figure 3 for ***CNTftt***. The curves subtend an area, indicating a capacitance. Pseudocapacitance induced by faradic reactions contributes to the capacitance, which depends on the (OH-) surface functionalization (see the FT-IR analysis above) of the carbon nanostructures (Pan at al., 2007). The redox reaction (faradic process) can be considered as follows (Pan et al., 2007):

$$>C\text{-}OH \rightarrow C=O + H^+ + e^-$$

$$>C=O + e^- \rightarrow >C=O^-$$

The specific capacitance can be calculated from the CV curve using the following equations $C=(It)/(2m\Delta V)$, where I is the average discharge current in the CV test (A), m is the mass (g) of active materials, ΔV is the potential window and t is the discharge time (s). Specific capacitances of 310, 298, 356 and 145 F/g were calculated from CV curve at 2 mV/sec for ***CNTp***, ***CNTf***, ***CNTftt*** and ***GO***, respectively. As could be expected the specific capacitance decreases up to an average of 18% with the increasing of scan rate, which originate from the internal resistance of the electrode. The very high value (Pan et al., 2007) obtained for ***CNTftt,*** is likely due to both the hydrophilic nature (the remaining functional groups improve the wettability of the CNT's surface, without affecting significantly the electrical transport of the electrode) and the high surface area (BET evaluated by nitrogen adsorption/desorption isotherm, not shown here) of 540 m^2/g due to combined contribution of micropores and mesopores. In particular, the sample shows a micropore volume of 0.49 cm^3/g, likely due to small inter-nanotubes surface porosity and a mesopore volume with a multimodal pore size

distribution (BJH (Barrett-Joyner-Halenda) pore distribution) centred at 2.5 nm (inner nanotube diameter), 16 and 30 nm (larger pores between nanotubes). The hierarchical construction due to the combination of micropores and mesopores provides the space for electric double layers and easy access channels for the electrolyte ions to the exterior and interior pore surface, the mesopores provide low resistant pathways for ion diffusion in the pores and a good charge propagation, the micropores play an essential role for the optimization of the electrical double-layer surface. In comparison, ***CNTp*** has a lower surface area of 380 m^2/g, whereas ***CNTf*** shows increased surface area of 595 m^2/g, but excessive functionality. Finally, the capacitance value of 145 F/g is consistent with the ***GO*** functionalized structure and its surface area of 230 m^2/g .
It is not possible to exclude the effect of cobalt nanoparticles, contained in the core of the nanotubes, on the capacitive performance of the electrodes. On the other hand, cobalt constitutes less than 10 wt.% of the samples (Thermogravimetric-based evaluation), while, typically, supercapative peaks are not observed when the metals are carbon coated (Ang et al., 2004, Lee et al., 2011). In any case, the subsequent ***CNTp*** treatments result in a slight further reduction of cobalt amount in the sample ***CNTftt*** which has the highest capacity. Further investigations are in progress to clarify this aspect, even making comparisons with nanotubes almost completely purified. It is a complex topic, indeed more intense treatments affect carbon structure too.

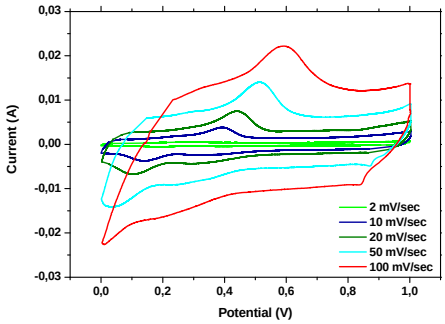

Figure 3: Cyclic Voltammetry curves of CNT in 1M H_2SO_4 aqueous solution.

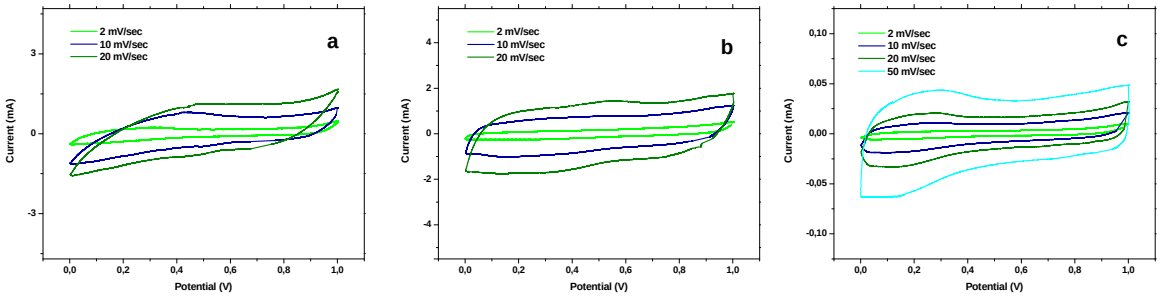

*Figure 4: Cyclic Voltammetry curves of **CNTf** (a), **CNTftt** (b) and **GO** (c) in NaCl 1mg/l solution as electrolyte.*

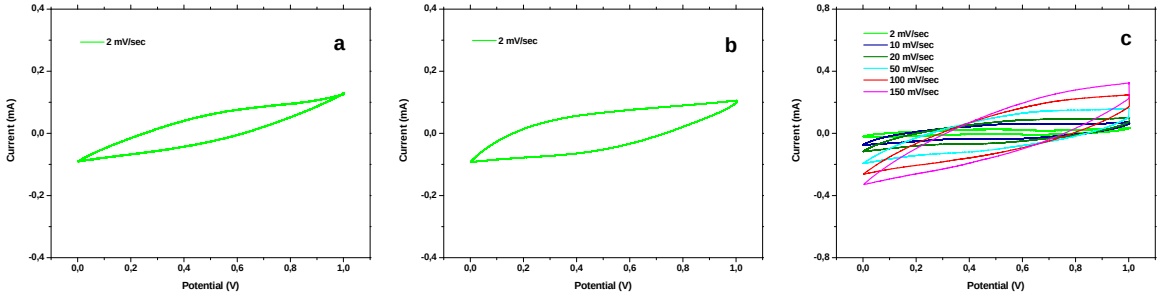

*Figure 5: Cyclic Voltammetry curves of **CNTf** (a), **CNTftt** (b) and **GO** (c) in As(III)+ As(V) 1mg/l solution as electrolyte.*

In addition, CV was performed to check the electrochemical activity of ***CNTf***, ***CNTftt*** and ***GO*** in NaCl containing water electrolyte (Figure 4). The capacitance of ***CNTf***, ***CNTftt*** and ***GO***, as expected, results lower

than that obtained in the aqueous electrolyte. On the other hand, high capacitance values were also measured for ***CNTf*** and ***CNTftt***, (135 and 189 F/g at 2mV/sec, respectively), a capacity of 85 F/g was measured for ***CNTp***. These results are in agreement with the behaviour reported in (Mishra et al., 2011a, Mishra et al., 2011b). They concluded that the presence of the surface functional groups create the intermediate bonding between water molecules and CNTf surface providing better contact between electrode and electrolyte, leading to high capacitance due to small distance between the electrode interface and electrolytic ions. Moreover, we also demonstrate that a structure electrically more preserved allows to obtain higher performance.

CV was also performed to check the electrochemical activity of ***CNTf***, ***CNTftt*** and ***GO*** towards arsenate and arsenite ions. The capacitance values measured in arsenite and arsenate electrolyte solution, at 2mV/sec, see Figure 5, for ***CNTf***, ***CNTftt*** and ***GO*** result equal to 140, 184 and 40 F/g. The samples behavior are thus quite close to that exhibited in NaCl electrolyte.

4. Conclusion

The simplicity of CDI makes this approach very attractive as an alternative method to more classic approach for both static and mobile water desalination and purification applications. We measured for our samples very high capacitances values both in H_2SO_4 and in ion salts electrolytes. The measured capacitances are in the order CNTftt>CNTp>CNTf>GO in H_2SO_4 and CNTftt>CNTf>CNTp>GO in arsenite/arsenate and NaCl electrolytes.

Reference

Acik M., Lee G., Mattevi C., Chhowalla M., Cho K., Chabal Y. J., 2010, Unusual infrared-absorption mechanism in thermally reduced graphene oxide, Nat. Mater., 9, 840–845.

Ang K. H., Alexandrou I., Mathur N. D., Amaratunga G. A. J., Haq S., 2004, The effect of carbon encapsulation on the magnetic properties of Ni nanoparticles produced by arc discharge in de-ionized water. Nanotechnology, 15, 520-524.

Baldino L., Sarno M., Cardea S., Irusta S., Ciambelli P., Santamaria J., Reverchon E., 2015, Formation of Cellulose Acetate - Graphene Oxide Nanocomposites by Supercritical CO_2 Assisted Phase Inversion, Ind. Eng. Chem. Res., 54, 8147−8156.

Benson J. , Kovalenko I., Boukhalfa S., Lashmore D., Sanghadasa M., Yushin G., 2013, Multifunctional CNT-Polymer Composites for Ultra-Tough Structural Supercapacitors and Desalination Devices, Adv. Mater., 25, 6625–6632.

Ciambelli P., Sannino D., Sarno M., Fonseca A., Nagy J.B. 2005, Selective formation of carbon nanotube over Co-modified beta zeolite by CCVD. Carbon, 43, 631-640.

Ganguly A., Sharma S., Papakonstantinou P., Hamilton J., 2011, Probing the Thermal Deoxygenation of Graphene Oxide Using High-Resolution In Situ X-ray-Based Spectroscopies, J. Phys. Chem. C, 115, 17009–17019.

Lee S. J., Cho J.-H., Lee C., Cho J., Kim Y.-R., Park J. K., 2011, Synthesis of highly magnetic graphite-encapsulated FeCo nanoparticles using a hydrothermal process. Nanotechnology, 22, 375603 (7 pp).

Mishra A. K., S. Ramaprabhu, 2010, Magnetite decorated multiwalled carbon nanotubes based supercapacitor for arsenic removal and desalination of seawater. J. Phys. Chem. C, 114 2583–2590.

Mishra A. K., Ramaprabhu S., 2011a, The role of functionalized multiwalled carbon nanotubes based supercapacitor for arsenic removal and desalination of sea water, J. Exp. Nanosci., 7, 85-97.

Mishra A. K., S. Ramaprabhu, 2011b, Functionalized graphene sheets for arsenic removal and desalination of sea water, Desalination, 282, 39-45.

Pan H., Poh C.K., Feng Y. P., Lin J., 2007, Supercapacitor Electrodes from tubes in tube carbon nanostructure, Chem. Mater., 19, 6120-6125.

Porada S., Zhao R., van der Wal A., Presser V., Biesheuvel P.M., 2013, Review on the science and technology of water desalination by capacitive deionization, Prog. Mater. Sci., 58, 1388–1442.

Sarno M., Sannino D., Leone C., Ciambelli P., 2012, Evaluating the effects of operating conditions on the quantity, quality and catalyzed growth mechanisms of CNTs, J. Mol. Catal.- A Chem., 357, 26-38.

Sarno M., Tamburrano A. Arurault L., Fontorbes S., Pantani R., Datas L., Ciambelli P., Sarto M.S., 2013a Electrical conductivity of carbon nanotubes grown inside a mesoporous anodic aluminium oxide membrane, Carbon, 55, 10-22.

Sarno M., Senatore A., Cirillo C., Petrone V., Ciambelli P., 2013b, Oil Lubricant Tribological Behaviour Improvement Through Dispersion of Few Layer Graphene Oxide, J. Nanosci. Nanotechnol., 14, 4960-4968.

Zhao R., Porada S., Biesheuvel P.M., van der Wal A., 2013, Energy consumption in membrane capacitive deionization for different water recoveries and flow rates, and comparison with reverse osmosis, Desalination, 330, 35-41.